Technical Report TR17OCT03

University of Pennsylvania
Center for Sensor Technologies
Philadelphia, PA 19104

SUNFEST REU Program

Remote Cognosensors: Developing an NIR Imaging Model to Map Brain Function

NSF Summer Undergraduate Fellowship in Sensor Technologies
Prasheel Lillaney, Department of Bioengineering, University of Pennsylvania
Advisor: Dr. Britton Chance

ABSTRACT

Near-infrared (NIR) imaging has provided new insight into optical imaging of human tissue. The purpose of this study is to develop an NIR imaging system that could potentially be used to study cognitive function by measuring the optical parameters (μ_a and μ_s`) of the human prefrontal cortex. The desired system should be a remote sensing system that does not need direct contact with the subject. It should also be able to work over a distance of 50 cm to 2 m from the subject. This study presents a method of remote sensing via a time resolved spectroscopy approach. Two methods of analysis are used: a single photon counting (SPC) method; and the second being a series of gated integrating circuits (Box Car). System design and initial results are shown for both systems. Actual photon migration patterns, from which values of μ_a are calculated, were obtained via the SPC method over a distance of 60 cm. Also, experimental results demonstrating pulse shaping are shown from the Box Car system. Finally, noise level reduction in the SPC method is taken into consideration, along with an option for achieving correct Box Car gate timing.

Table of Contents

1. INTRODUCTION

Human brain function imaging plays a crucial part in determining how the brain works under different conditions. Using techniques such as magnetic resonance imaging and computed tomography scans, it is possible to see different areas of the brain "activate" as a test subject is asked to solve a puzzle or recognize a familiar face. Another technique uses near-infrared (NIR) imaging to try to determine the optical parameters μ_a and $\mu_s`$, which have been shown to correlate to blood volume and oxygenation in human tissue [1].

One of the current NIR methods uses a multi-source, multi-detector array placed in a plastic holder. The holder itself is held in place over the forehead with the use of Ace bandages and Velcro straps. As a result when the subject moves his forehead the placement of the source/detector network shifts slightly relative to the subject's forehead. These movements lead to outlier signals and questions about the reproducibility of the experiment, mainly how well the source/detector array can be replaced over hundreds of trials [2].

Two ideas have been proposed to avoid these problems with head movement during testing. The first minimizes the electronic devices that would be attached to the subject's forehead. Complementary metal-oxide semiconductor (CMOS) technology could be used to minimize the detectors to about the size of a quarter. The detectors could then be placed in any fashion around a central light source (see Figure 1). The whole configuration could be held in place with one bandage tied around the head, and any motion artifacts found in the previous system would be minimized. The detectors would then transmit the data to a remote source where they could be monitored [2].

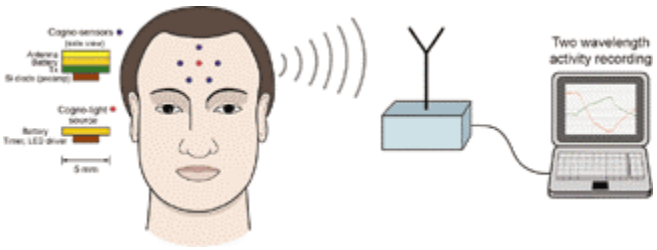

Figure 1 – The small light source is denoted in red and the detectors are shown in blue. The whole system transmits data to a remote source shown to the right [2].

In the second approach, the source and detector are placed anywhere from 50 cm to several meters from the subject. The source is focused through a lens onto the subject. A Fresnel lens then captures the reflected and diffuse photons and focuses them onto a photomultiplier tube (PMT). In this setup, the source would be placed at approximately a 10-degree angle with respect to the subject [2].

This paper will address the design and testing of the above non-contact system. The following sections will focus on the background pertaining to the analysis of the

PMT signal, the design and layout of the non-contact system, experimental results, conclusions, and recommendations for future work.

2. BACKGROUND

2.1 Time Resolved Spectroscopy (TRS) and Time Correlated Single Photon Counting

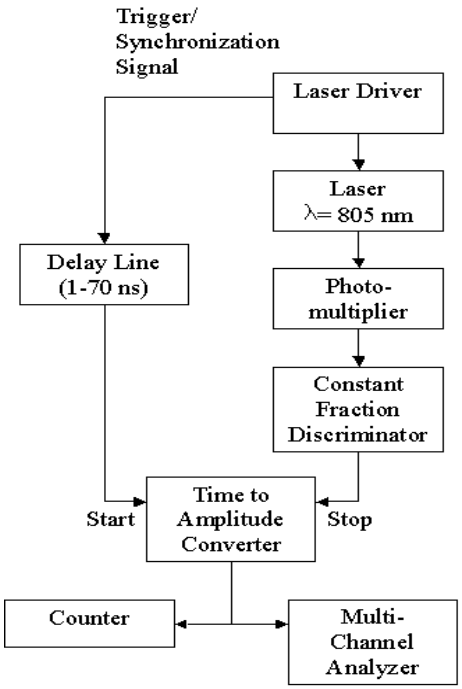

Figure 2 - This is a block diagram for the TRS system showing the progression of the signal through the different components. The CFD, TAC, and MCA can all be bought on an integrated board that can be inserted into a PC so that the photon migration pattern can be displayed in real time as the voltage from the TAC is put into memory by the MCA.

The initial approach used to analyze the PMT signal will be a Time Correlated Single Photon Counting method. The basic principle is that for every pulse from the laser many photons are released into the subject. The job of the PMT, Constant Fraction Discriminator (CFD), and Time to Amplitude Converter (TAC) system is to measure the amount of time each photon takes to arrive at the detector (PMT) with respect to the original excitation event. Once the optical signal arrives at the photo-cathode of the PMT, it triggers the release of electrons that are then cascaded down a series of dynodes to amplify the signal. The signal then arrives at the anode and is then fed into the CFD. The time that it takes the signal to travel from the photo-cathode to the anode is known as the transit time, and as this time becomes shorter the time resolution of the whole system increases [3].

The PMT signal that comes out of the anode still has considerable amplitude jitter and as a result must be sent to the CFD. The CFD creates a constant amplitude pulse for every PMT pulse that is over a certain minimum voltage. The CFD accomplishes this via a system of delays and inverters [see Appendix A]. The data from CFD is then fed into the stop input of the TAC, while the trigger signal from the laser driver is fed into the start input after it travels through a variable delay line. The TAC starts a voltage ramp when it receives the start signal and stops the voltage ramp when it receives the stop signal. Thus the TAC directly correlates time to voltage [see Appendix B]. The output of the TAC is fed into a counter, mainly to check whether the signal is reasonable, and into a multi-channel analyzer (MCA). The MCA converts the output voltage of the TAC into a histogram that displays photon counts versus time (ns), where the time corresponds to how long it took the PMT to detect a photon relative to the time of laser excitation. The photons that diffused farther into the subject would take a longer time to be detected, and as a result the histogram would show a photon migration pattern.

The slope of this photon migration is directly related to the absorption coefficient (μ_a) by the Patterson-Chance-Wilson equation ($\mu_a * c$ = slope, where c is the speed of light) [2].

2.2 Continuous Wave (CW) Cognosensor

Previous work has shown that NIR imaging offers insight into muscle activation and, more importantly, cognitive function. Several systems have used the continuous wave (CW) model, where a constant intensity of light is put into the tissue and the intensity of light leaving the surface of the tissue is recorded [4]. In experiments focusing on skeletal muscle activation resulting from increased load, it was shown that the 730 nm NIR signal decreased because of increased deoxy-hemoglobin (Hb), whereas the 850 nm NIR signal increased because of decreased oxy hemoglobin (HbO_2). Furthermore, once the exercise was stopped the signals began to approach their original values as a result of re-oxygenation (see Figure 3).

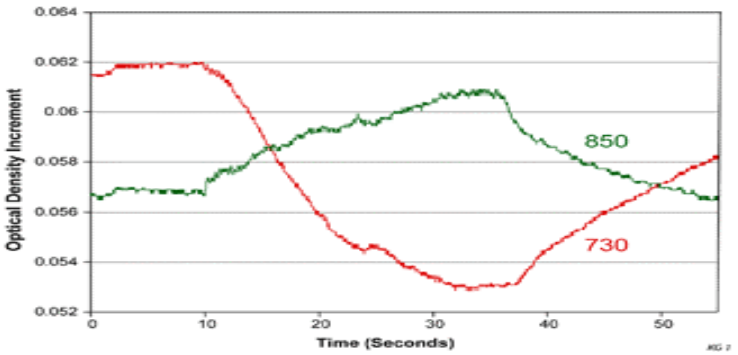

Figure 3 – Illustration of 730, 850 nm NIR signals of skeletal muscle during exercise [5].

Other NIR experiments done with similar instrumentation have shown interesting signals relating to subject behavior. Histograms can be created for numerous positions on the subject's forehead, and data can be collected on activation in those areas over a large number of trials. Interestingly, it has been shown that when a subject lies there is far more activation than when the subject is telling the truth (see Figure 4). It is important to remember, however, that since different people have different characteristic activation patterns results cannot be compared across subjects [2].

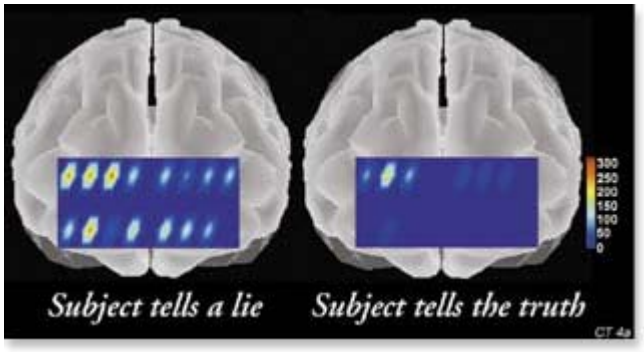

Figure 4 – Illustration of the fact that there is more activation in the prefrontal cortex when a subject lies when compared to the response when the subject tells the truth [2].

2.3 TRS Contact Sensor

The obvious question that arises about the non-contact system is not whether it is possible to get signals similar to those shown above, but whether the system is sensitive enough to detect changes in the optical parameters for a dynamic system such as human tissue. This difficult question can be partially answered by results from a previous TRS contact model (see Figure 5). In this setup the signal from the detector was fed into a single photon counting system (SPC) that had all the components integrated on to one board. The board had two inputs, one for the detector signal and the other for the trigger signal from the source, which in this case was a 780/830nm, 40μW laser driven at 5 MHz. Results from the experiment demonstrated that quantification of absorption changes were accurate to 10^{-3} cm^{-1} with sensitivity to 10^{-4} cm^{-1}. Moreover, these results were mainly limited by laser instability [6]. The task remains to replicate these results for the remote condition, but at least it is known that the TRS system can provide the above-mentioned degree of sensitivity and accuracy.

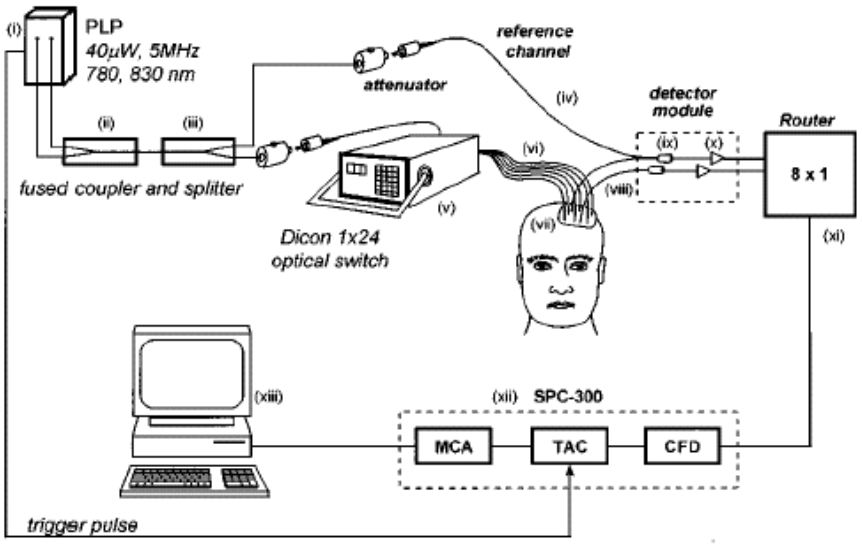

Figure 5 - The laser source is shown to the top left of the diagram. It is fed into the optical switch allowing for variation of source position on the subject's forehead. The detector signal is then fed into the SPC-300 board shown to the bottom right. The results from the multi-channel analyzer (MCA) on the board can be displayed o a PC [6].

2.4 Proposed Model

The model that will be used to carry out the experiment will have the subject at a distance of approximately 50 cm from the source and detector. The source will be put at an angle of roughly 10 degrees with respect to the detector. Focusing the source through a lens is optional and will be done if the signal on the detector side is too weak to recognize. The detector will be placed 10-15 cm behind a Fresnel lens, which will collect the diffuse photons returning from the subject and focus them onto the PMT fiber. The signal from the PMT will be fed into either a TRS system or a Box Car detector (see Figure 6) . (Additional details are provided in section 3.)

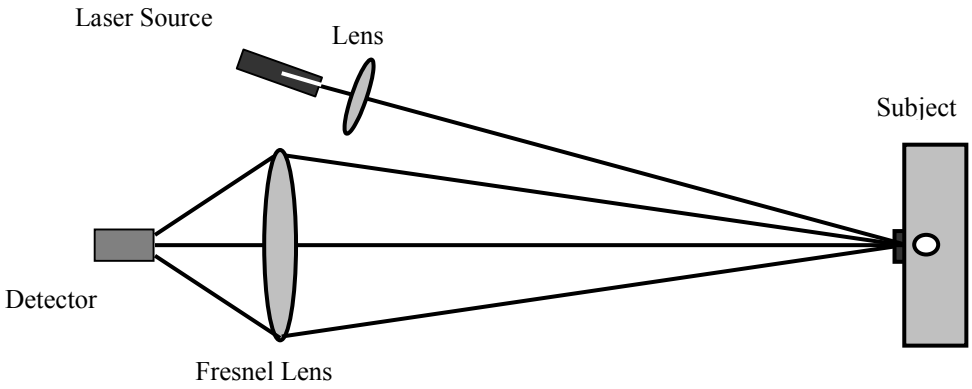

Figure 6 – Illustration of detector/source positioning with respect to the subject

3. SYSTEM DESIGN

3.1 Analysis by Conventional TRS

The TRS system design is fairly similar to that shown in the background section, with a few variations. The driver used is a Hewlett Packard 8082A Pulse Generator on a frequency range of 5 to 50 MHz. The amplitude and FWHM (Full-Width, Half-Maximum) of the pulses are below 1.0 V and 5.0 ns, respectively. It is optimal to minimize the FWHM of the driver so that the instrument response function in the result is also minimized (for further discussion, see section 4). The signal from the driver is split

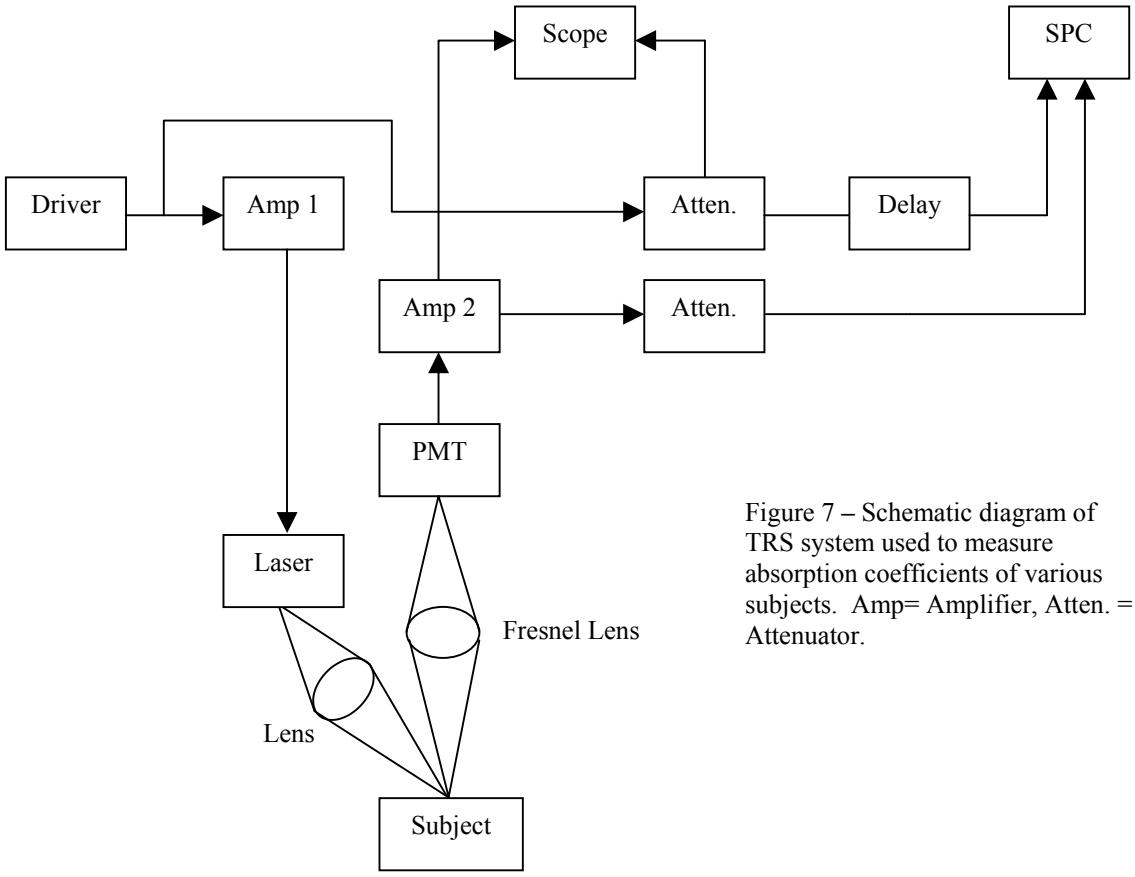

Figure 7 – Schematic diagram of TRS system used to measure absorption coefficients of various subjects. Amp= Amplifier, Atten. = Attenuator.

into an amplifier and an attenuator. The amplifier (Amp 1) used is a Mini-Circuits Monolithic Amplifier (Model HELA-10b) with 12 dB typical gain and 20 dBm (6.3 V p-p for 50-Ω impedance) max power rating at input. This amplifier feeds the driver signal into the laser (780 nm) for a typical optical power output of approximately 1.2 mW. The two attenuators used are identical and are variable from 1 to above 40 dB attenuation, with 1 W max input power and 50-Ω impedance at input. They are used to keep the signals being fed into the SPC 300 board below 80 mV p-p, so the attenuation used can range from 10 to 15 dB. The SPC board, purchased from Edinburgh Instruments Ltd, creates the photon migration pattern and displays it on a PC. The attenuator used for the driver signal is fed into a variable delay line (1-70 ns delay via coaxial cable with 20 ps accuracy) before it enters the SPC board, so that the position of the photon migration pattern can be shifted to allow complete visualization of the photon decay.

The PMT used in the system is a Hamamatsu R5600U and is operated in the 800 V range. The PMT signal is fed directly to a Hamamatsu C5994 amplifier (Amp 2), which is made especially for use with PMT signals (10 dBm max power input, 36 dB gain, 50 KHz to 1.5 GHz frequency range). The signal from this amplifier is split into two. One half goes to an attenuator and eventually to the SPC board. The other half is monitored on the oscilloscope in order to make sure that there is a live PMT signal during testing. It may seem odd that the PMT signal is being amplified and then immediately attenuated before entering the SPC board. The design is set up this way because the SPC board is very sensitive to PMT signals and can create photon migration patterns with a PMT signal that is less than 5 mV. Yet, it is difficult to monitor such a small signal on the oscilloscope. As a result the signal must be amplified first so that it can be monitored, but then attenuated at the next step so that the SPC board does not overflow. The cables used to connect all the components are coaxial BNC cables with 50-Ω impedance. Finally, a 6.5-inch diameter Fresnel lens is placed 10-15 cm in front of the PMT fiber in order to capture the optical signal from the subject and focus it onto the fiber. Another lens maybe used in order to focus the laser source if deemed necessary. (see Figure 7).

3.2 Analysis by Box Car Detectors

The TRS system mentioned above is limited by the pulse pile-up distortion. These errors create an upper limit of 0.1 for the ratio of detected photons to the number of excitation events from the laser. For higher values of this ratio mathematical corrections to the data must be made to remove the error [3]. In order to avoid this problem of having an upper limit placed on the number of photons that can be detected, the Box Car detector system can be used instead of the SPC 300 board.

The principle of the Box Car system relies on the concept of gated integrators (see Figure 8). The integrators being used are simple resistor capacitor networks (R_1, C_1, R_2, C_2, R_3) and are on a timing schedule, which is controlled by a series of delay lines, flip-flops (F.F.), and pin diodes. For example, the first gate is turned on when the impulse from the pulse generator arrives at the first flip-flop. At this point the flip-flop transmits

the pulse to the pin diode in front of the first integrator. Up to this point the pin diode was acting like a closed switch, but upon receiving the impulse from the pulse generator it conducts current and acts as a closed switch. As a result the signal from the PMT is allowed to travel across the pin diode and enter into the first integrator.

The integrator then reports a DC voltage to the first channel of the analog-to-digital converter, which is then stored to memory. Hence, the pulse generator was simply

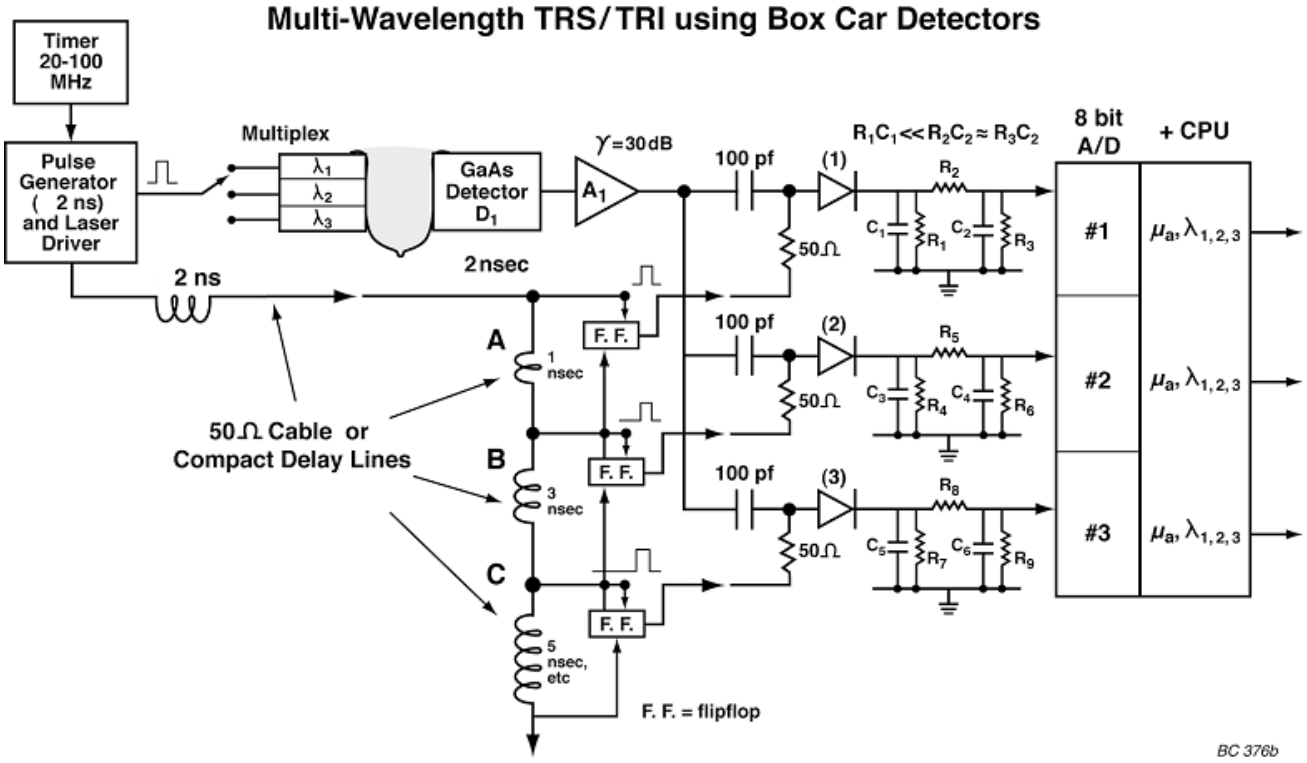

Figure 8 – Illustration of Box Car detector system. #1,2,3 stand for gate 1,2,3 and so forth. The element before each resistor, capacitor integrator is a pin diode. F.F stands for flip-flop and GaAs detector (D_1) shown is a Gallium-Arsenide PMT.

acting as a "platform" for the PMT signal to be integrated upon. In order to turn off the first integrator, the original impulse from the pulse generator is also fed though delay line A (shown here as 1 ns). After traveling through the delay line the impulse arrives at the second input of the flip-flop. Once the flip-flop receives the second delayed impulse from the pulse generator it no longer transmits any signal. As a result the pin diode again acts as a closed switch, and the first integrator is turned off. Yet, the same pulse that arrives after a 1 ns delay to the second input of the first flip-flop now arrives at the first input of the first flip-flop and turns on the second integrator according to the same principle. The second flip-flop receives a second input after a 3 ns delay (delay line B). This process can go on for as many gates as needed to reconstruct the logarithmic decay curve in order to measure the absorption coefficient of the subject. The delay lines get longer for the sequential gates because the PMT signal is also getting weaker, and in order to preserve equal signal to noise ratio across all the gates the integration time must increase for the later gates (see Figure 8).

The major drawback to the system is the difficulty of finding a flip-flop or other logic device with a response time that can handle the 1 and 3 ns timing needed to run the first few gates. The advantages to the system, on the other hand, are considerable. First, the problem of pulse pile-up can be avoided, since the system is not using a conventional SPC approach. Next, the system can be miniaturized and replicated for as many gates and channels as are needed. For example, it is feasible to have a 3-wavelength source, 8 detectors, and multi-position scanning system via Box Car analysis. It should be noted that Figure 8 shows the system in a contact breast imager model, but it can easily be interchanged with the non-contact NIR cognosensor system. [Note: All Box Car specifications credited to Chance Lab].

4. EXPERIMENTAL RESULTS

4.1 TRS Results

The following data were recorded with the SPC 300 board for various remote distances of approximately 60 cm from the source/detector system with a high voltage of approximately 900 volts applied to the PMT. Figure 9 shows a linear plot of photon counts versus time across three trials. The first two trials were performed with the subject (phantom 1) in a position to minimize the specular reflection response. Trial 3 was performed with a slight change of angle on the phantom to increase the reflective response.

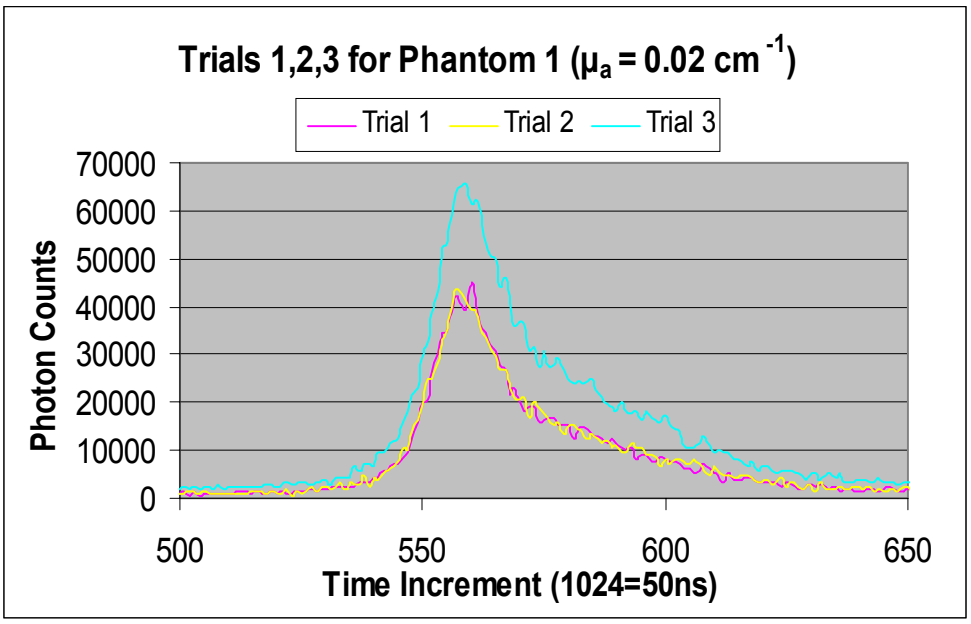

Figure 9 – Graph of photon counts versus time for Phantom 1 at a remote distance of 60 cm.

Figure 10 shows the same data as above except with the y-axis changed to a logarithmic scale. At time = 575 the reflection has ended, and the true photon migration pattern is seen.

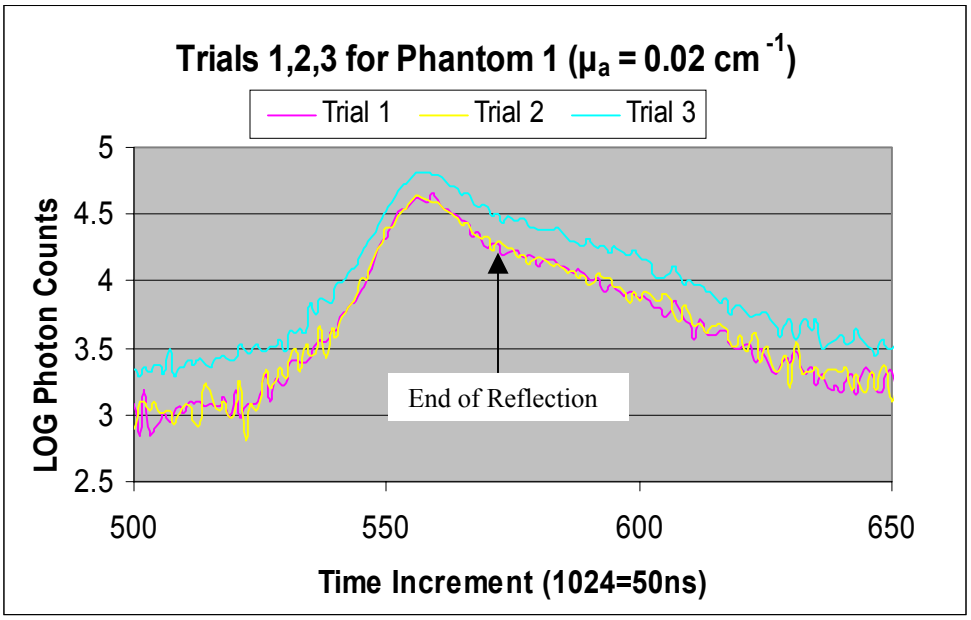

Figure 10 - Graph of log photon counts versus time for Phantom 1 at a remote distance of 60 cm.

Data points 575-625 were used to fit via regression and determine the slope of the logarithmic decay for the photon migration pattern (see Figure 11). Only trial 1 is shown in the figure for convenience (statistics on trial 1 and other two trials are in Appendix C). Converting the decay slopes across all three trials into absorption coefficients yields an average μ_a of 0.01387 cm $^{-1}$ ± 4.7% (95% confidence).

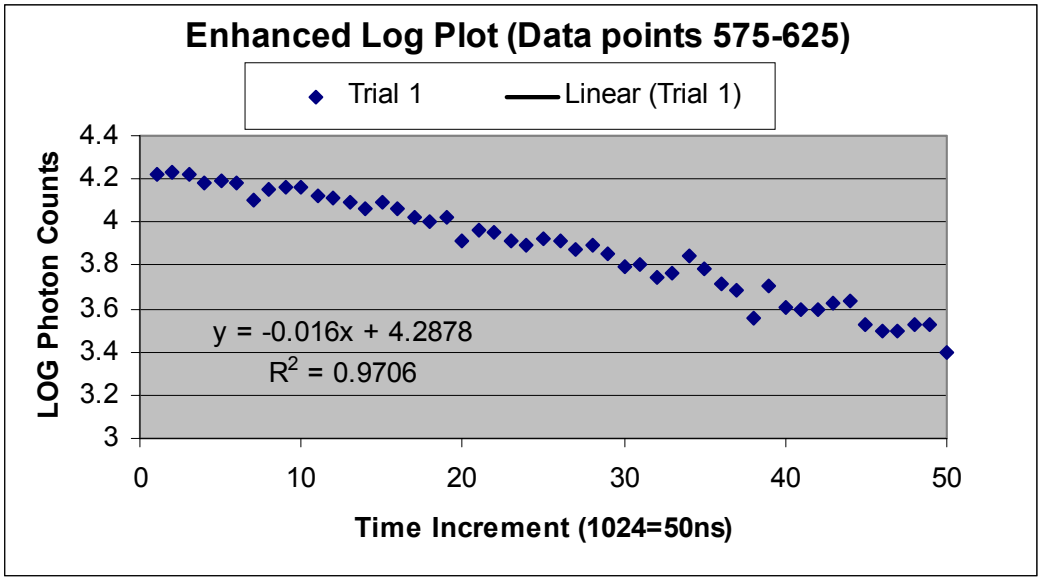

Figure 11 – Selected points for log plot of trial 1 used to perform regression analysis.

The above three trials displayed that the photon migration pattern and specular reflection from Phantom 1 flowed into each other, meaning that there was no time difference between the two responses. However, by changing the attenuation value on the PMT signal entering the SPC 300 board, increasing the PMT voltage to near 1100

volts, and changing to a much higher absorption phantom (μ_a= 0.37 cm $^{-1}$), it was possible to separate the two signals (see Figure 12). The signal was too noisy, however, to perform regression analysis (the standard error of slope was greater than 10%). This problem is discussed further in section 5.

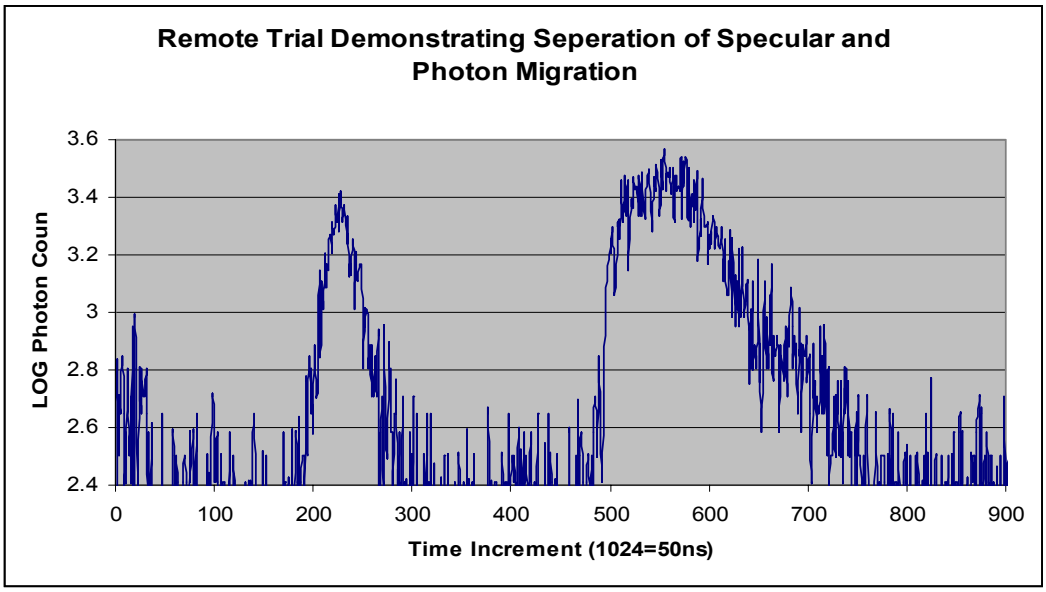

Figure 12 – Graph of separation of specular reflection and photon migration pattern when attenuation, PMT voltage, and phantom was changed.

4.2 Initial Box Car Results

Although no flip-flop or logic device was found that was fast enough to handle the timing controlling the gates in the Box Car system, it was still possible to design a 1-gate integrator without the pin diode, delay line, and flip-flop timing system. Figure 13 demonstrates the voltage dampening out of the output of the integrator (R_1= 50 – Ω, C_1= 100 pF, R_2= 50 – Ω, C_2= 3 nF, no R_3 used) when a 1 V p-p impulse was sent through at various frequencies. The voltage was decreased by a factor of 10 at 5.2 MHz.

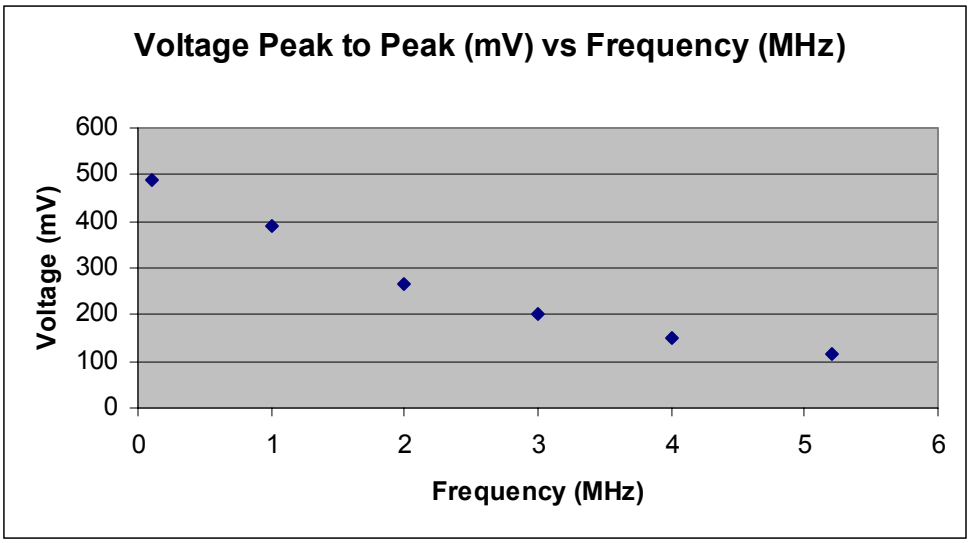

Figure 13 – Graph demonstrating voltage dampening out of 1 gated Box Car.

One of the main purposes of the Box Car system is to stretch the input pulses as they go through the integrator, making the result at the analog-to-digital converter more stable. Figure 14 demonstrates the above-mentioned pulse stretching. At a frequency of 5.2 MHz the input pulse had a FWHM that was 37% as long as the FWHM of the output pulse, thus showing a considerable amount of stretching.

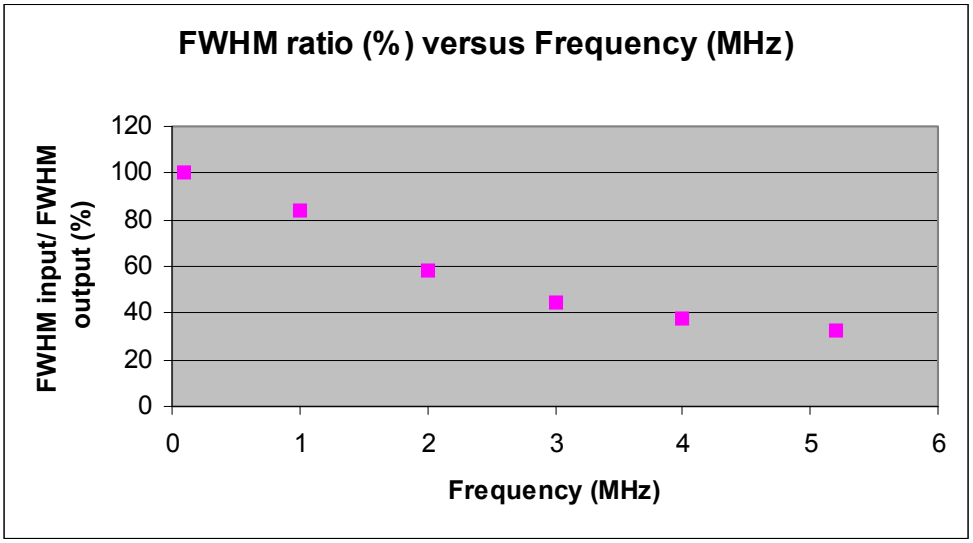

Figure 14 – Graph demonstrating pulse stretching out of 1 gated Box Car.

5. DISCUSSION AND CONCLUSIONS

The results from the TRS system for Phantom 1 (μ_a of 0.01387 cm $^{-1}$ ± 4.7%) show roughly 30% error from the actual value of 0.02 cm^{-1}. This error would suggest that perhaps the signal being analyzed for the decay slope is not the true photon migration pattern. However, it is important to remember that the signal measured by the SPC 300 board is a convolution of the true signal and another signal known as the instrument

response function. The instrument response function is a result of the pulse that is driving the source for the experiment (for this experiment, the Hewlett Packard 8082A Pulse Generator). Therefore, in order to measure an absolute value for μ_a the data must first be de-convolved, for which there are various methods [6]. Since it was shown in the results that it is perhaps possible to further separate the specular response and the actual photon migration pattern (see Figure 12), no steps were taken to de-convolve the data since it is not yet known which data set is optimal.

The results from the Box Car system demonstrated that pulses in the frequency range of 1-5 MHz could be handled with the 1-gated integrator in the appropriate fashion (see Figures 13 and 14). If frequencies of up to 50 MHz were applied, one would simply have to experiment with the values of C_1 and C_2 to achieve the appropriate pulse shaping for the analog-to-digital converter.

6. RECOMMENDATIONS

Although it was shown that data could be seen over remote distances with the TRS system, significant work is needed to optimize the system. First, further tests should be done to try to minimize the noise seen when the specular reflection and photon migration pattern are separated. If noise can be reduced, it will be possible to confirm that the second peak that appears is actually a photon migration pattern and not just an artifact from the SPC 300 board or from another component in the system. The first step should be to move the SPC 300 board to another PC and see if the same results can be obtained.

The Box Car system remains largely untouched. However, one option remains to achieve the nanosecond timing needed for the gates. It may be possible to program an emitter coupled logic (ECL) chip or purchase an ECL flip-flop that bhaves in the fashion needed to control the integrator gates.

7. ACKNOWLEDGMENTS

First, I would like to thank my project advisor, Dr. Britton Chance, for his encouragement, advice, and most importantly his patience. I would also like to thank Dr. Jan Van der Spiegel, the SUNFEST committee, the National Science Foundation, and the Microsoft Corporation for making it possible for undergraduates to pursue meaningful research projects. Lastly, I would like to give special thanks to Leonid Zubkov for developing the laser driver and Zhongyao Zhao and Xavier Intes for their technical expertise and advice with the TRS system.

8. REFERENCES

1- V. Ntziachristos, X. Ma, and B. Chance. Time-Correlated single photon counting imager for simultaneous magnetic resonance and near-infrared mammography. *Rev. of Sci. Instruments, Vol. 69, No. 12,* December 1998, pg 4221.

2- B. Chance, S. Nioka, and Y. Chen. Shining New Light on Brain Function. *OE Magazine,* July 2003, pg 16-19.

3- D.V. O'connor and D. Phillips. *Time~correlated Single Photon Counting.* Academic Press, London, 1984. Pg 103,164,165.

4- F.E.W. Schmidt. *Development of a Time-Resolved Optical Tomography System for Neonatal Brain Imaging.* Thesis submitted at University of London, November 1999. Pg 59,60, 102.

5- K. Gangavarapu, Q. Liu, H. Liu, J. Liu, S. Nioka, and B. Chance. *Future Applications of Nanotechnology in the Field of Functional Brain Imaging*. DOE Nanoscale Science Research Center Workshop, Feb. 26-28, 2003.

6- V. Ntziachristos, X. Ma, A. G. Yodh, and B. Chance. *Multichannel photon counting instrument for spatially resolved near infrared spectroscopy. Rev. of Sci. Instruments, Vol. 70, No. 1 ,* December 1999, pg 194, 200.

9. APPENDICES

Appendix A : CFD Principle

The CFD takes the input pulse from the PMT and splits it into two signals. The first signal is attenuated and the second is inverted and delayed. The pulses are then added together creating a bipolar signal that has a zero crossing level. The zero crossing level is then used by the CFD as the point to create the new impulse, which is independent of the original amplitude of the input pulse (see Figure A1). The CFD can also be set to reject any input pulses that have amplitudes falling outside a variable window. This setting allows for rejection of input pulses that are caused by double triggering or are part of the dark current of the PMT [4].

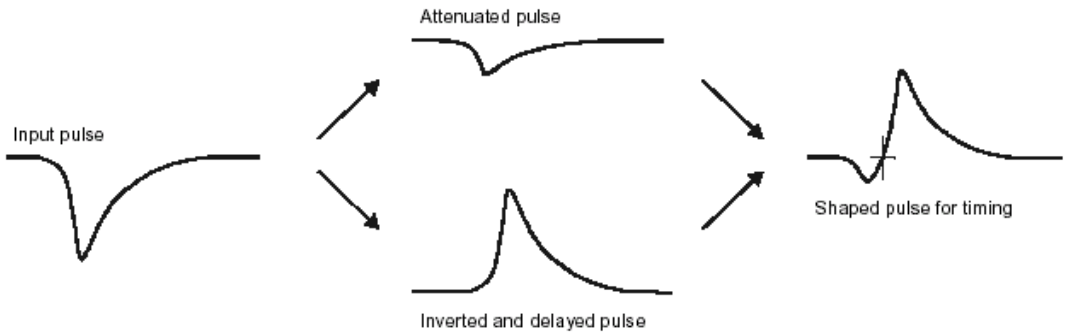

Figure A1 - Diagram of CFD timing principle [4].

Appendix B : TAC Principle

The TAC works with two inputs, a start input and a stop input. Once the TAC receives a start impulse it creates a voltage ramp (after a certain characterstic time delay inherent in the TAC being used). When the TAC receives the corresponding stop impulse it will stop the voltage ramp. Hence, the amplitude of the voltage ramp will be directly proportional to the time between the start and stop impules. Therefore the TAC takes time and directly correlates it to a voltage (see Figure B1).

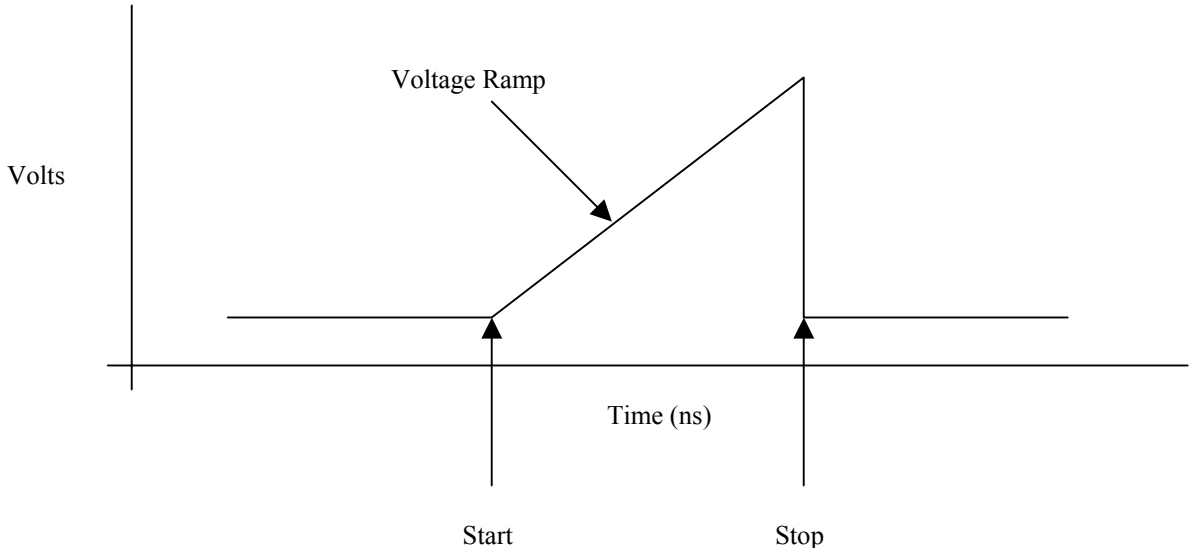

Figure B1 - Illustration of ideal TAC function when start and stop inputs are provided that are separated on the nanosecond time scale.

Appendix C : TRS Regression Analysis

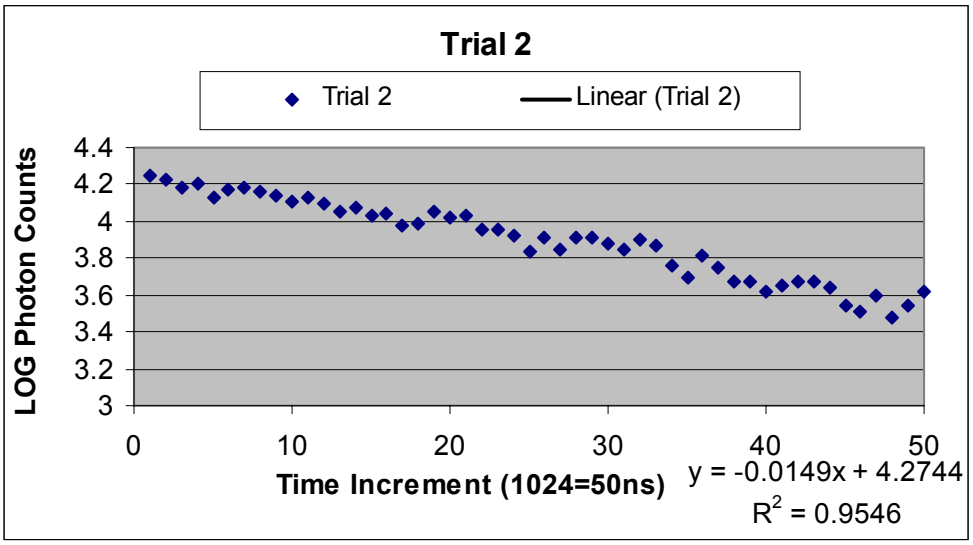

Figure C1 – Graph of points used to do regression analysis on Trial 2 for Phantom 1. Points 575-625 were used and the slope and R^2 value are listed to the bottom right.

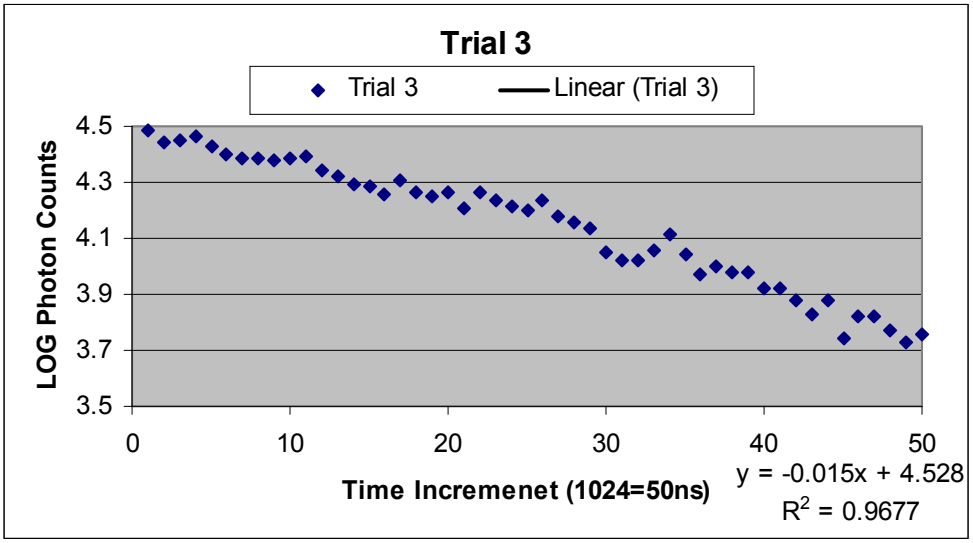

Figure C2 – Graph of points used to do regression analysis on Trial 3 for Phantom 1. Points 575-625 were used and the slope and R^2 value are listed to the bottom right.

Table C1 : Regression statistics for all three trials on Phantom 1.

Statistic	R^2 Value	Max Slope (95% CI)	Min Slope (95% CI)	Standard Error
Trial 1	**0.971**	**-0.01522**	**-0.01682**	**0.000398**
Trial 2	**0.955**	**-0.01392**	**-0.01578**	**0.000463**
Trial 3	**0.968**	**-0.0142**	**-0.01577**	**0.000391**